Rigid-compliant hybrid variation analysis using Monte Carlo interval approach for low-rigidity aircraft structure assembly

Biao Mei (biaomei@zju.edu.cn)
Zhejiang University https://orcid.org/0000-0002-6038-0370
Haijin Wang
Zhejiang University

Research Article

Keywords: Aircraft structure assembly, Ladder structure, Assembly variation modeling, Variation analysis, Monte Carlo interval approach

Posted Date: March 22nd, 2021

DOI: https://doi.org/10.21203/rs.3.rs-339802/v1

Rigid-compliant hybrid variation analysis using Monte Carlo interval approach for low-rigidity aircraft structure assembly

Biao Mei[1*], Haijin Wang[2]

1. Quanzhou Institute of Equipment Manufacturing, Haixi Institutes, Chinese Academy of Sciences, Quanzhou 362216, China

2. Institute of Advanced Technology, Zhejiang University, Hangzhou 310027, China

Corresponding author information:

Full name: Biao Mei;

E-mail address: biaomei@zju.edu.cn

Rigid-compliant hybrid variation analysis using Monte Carlo interval approach for low-rigidity aircraft structure assembly

Abstract To reduce downstream rework and design changes, variation modeling and analysis are indispensable in the assembly of complex products. In this paper, a rigid-compliant hybrid variation analysis method using the Monte Carlo interval approach is developed to assembly ladder structures, such as the skeleton of a horizontal stabilizer or a wing box. We first present the classical locating scheme of a low-rigidity aeronautical structure, and the contributors to the assembly variation of a ladder structure comprising locating errors and part geometric errors. Assembly variations induced by rigid-body locating errors and part geometric errors are mathematically modeled with rigid-body kinematics and the mechanistic method based on the Finite Element Analysis, respectively. And then, the two types of assembly variations are integrated into a rigid-compliant hybrid variation model. Probability distributions of the contributors are often unknown, especially in aircraft manufacturing with low production volume. Therefore, a novel variation analysis method using the Monte Carlo interval approach is proposed to compute the assembly variation, represented in the form of interval structural parameters. The assembly case of a scale wing skeleton shows the proposed rigid-compliant hybrid variation analysis method is efficient in the assembly variation analysis for low-rigidity aircraft structure.

Keywords Aircraft structure assembly, Ladder structure, Assembly variation modeling, Variation analysis, Monte Carlo interval approach

1. Introduction

The assembly of the low-rigidity structure is widely used in furniture-making, automotive, and aircraft industries. A real assembly system is often not coincident with its nominal mathematical model regarding the shape and location (position and orientation) of the fixtures and assembled parts, which induces the dimensional variation of the assembly. The assembly variation significantly affects the quality of the final product. To reduce downstream rework and design changes, realistic and accurate variation modeling and analysis are extremely needed in automobile and aircraft assembly.

In the past two decades, many achievements in rigid and compliant assembly variation models of 3D products have been obtained. In rigid models, assembled parts are treated as rigid-body. The assembly variation is estimated using rigid-body kinematics and homogeneous transformations[1-3]. Huang et al. [4] developed the stream-of-variation analysis (SOVA) model for 3D rigid-body assemblies for a single assembly station, in which kinematics errors related to part mating features and fixture locating errors are analyzed. However, no part deformation is included. For analyzing variation propagation in a multistation assembly process, the data-driven SOVA model is used and further improved by Huang et al. [5], in which the assembly process is modeled with a state transition dynamic system. Liu et al. [6] developed a generic state space approach to model 3D rigid-body variation propagation induced by various variation sources in multistation assemblies.

In complaint models, assembled parts are assumed to be deformable. Due to part geometric errors, gaps often exist between the mating features of the assembled parts. To close the gaps, clamps and fixtures are often used to clamp one part onto another part. The clamping process introduces assembly force and finally causes spring-back after assembly. Thus assembly variation is commonly predicted by the mechanistic method based on Finite Element Analysis (FEA) in compliant models. Liu and Hu [7] developed a mechanistic assembly variation model integrating the FEA with Method of Influence Coefficient (MIC) for the variation analysis of a complex flexible assembly. As an alternative, components geometric covariance is accompanied by principle component analysis for the variation analysis of a flexible assembly[8]. In literature[9], an assembly variation analysis scheme using datum flow chain, commercial variation analysis software, and the FEA is presented for complex assemblies. The impact of many factors on assembly variation such as different joint types[10], material characteristic[11, 12], welding sequence[13], riveting[14], misalignment[15], gap and gap closure[16, 17], and fixture design[18] are widely studied. In literature[19-22], the propagation of assembly variation is studied for automotive body and wing panel manufacturing.

In literature, the effects of rigid-body errors and part geometric errors on assembly variation are often analyzed separately. In rigid models, only the impact of rigid body errors on assembly

variation is focused on, while just part geometric errors are paid to in compliant models. However, in a 3D complex assembly of the low-rigidity structure, both types of errors may simultaneously contribute to assembly variation. This paper develops a rigid-compliant hybrid model for the variation analysis of the low-rigidity aircraft structure assembly. The contributors to the assembly variation of a ladder structure are first discussed. Since panels will be installed onto the ladder structure skeleton in the assembly of a horizontal stabilizer or a wing box, the assembly variation component along the normal of the mating surfaces between the panels and the skeleton is of paramount importance. This assembly variation component is affected by the locating errors of spars and the deformation of ribs. Assembly variations induced by rigid-body locating errors and part geometric errors are modeled with kinematics and mechanics, respectively, and integrated into a unified assembly variation model. When modeling the assembly variation related to part geometric errors, part deformation is characterized by warping or torsion angle instead of point deviations, which reduces the FEA's complexity.

If the contributors to assembly variation can be treated as random variables following certain probabilistic distributions, variation analysis can be executed with the Monte Carlo simulation (MCS) using the developed assembly variation model. It is widely and successfully used in automobile manufacturing. However, there is a big gap between annual productions of automobile and aircraft (several millions vs. a few hundreds)[23, 24]. The available information of part geometric errors and locating errors is often not enough to make the assumptions of their probability distributions, which is particularly evident in the prototype development stage. Moreover, in industrial production, the known information of some contributors to assembly variation is sometimes actually their tolerance intervals rather than probability distributions. For handling these problems, a general variation analysis method using the Monte Carlo interval approach is proposed for different types of variation sources, including probabilistic and non-probabilistic ones. In the proposed method, assembly variation is given in interval structural parameters instead of mean and standard deviation.

The remainder of the paper is organized as follows: In Section 2, the contributors to the assembly variation of a ladder structure are discussed. In Section 3, assembly variations induced

by rigid-body errors and part geometric errors are modeled with kinematics and mechanics, respectively. The rigid-compliant hybrid variation model is also established in this section. In Section 4, a general variation analysis method using the Monte Carlo interval approach is proposed for dealing with the situation that probability distributions of partial or entire input parameters for assembly variation analysis are unknown. To verify the effectiveness of the proposed assembly variation analysis method, a case study of a simulant wing skeleton is presented in Section 5. Conclusions are drawn in Section 6.

2. Contributors to assembly variation of the ladder structure

The ladder structure assembly is widely used in the aerospace industry, such as the skeletons of horizontal stabilizer and wing box. To ensure the finished product's quality, variation analysis is indispensable in the assembly process design stage. In this section, the contributors to the assembly variation of a ladder structure are discussed.

2.1 The classical locating scheme of a low-rigidity structure.

A rigid body has six degrees of freedom. The motion can be represented by six parameters, including three linear motions X, Y, Z and three rotations α, β, γ. The body's location (position and orientation) is assumed to be fully constrained when the six parameters are known with respect to the reference coordinate system. Meanwhile, the over-constrained N-2-1 (N≥4) principle is used to locate a low-rigidity structure considering the structure deformation. And the maximal projective plane of the low-rigidity structure is often redundantly located in practice.

The classical locating scheme of a low-rigidity structure is shown in Fig. 1(a). The locating fixture of the structure is abstracted to four locating blocks, one locating hole, and one locating slot. The blocks are distributed on the maximal projective plane of the structure, which restrains the out-of-plane motions, consisting of the translation along the plane's normal direction (Z-axis) and the rotations about the two axes of the plane (X- and Y-axis). The hole and slot are used to restrain the structure's motions in the maximal projective plane, including the translations along the X- and Y-axes and the rotation about the Z-axis.

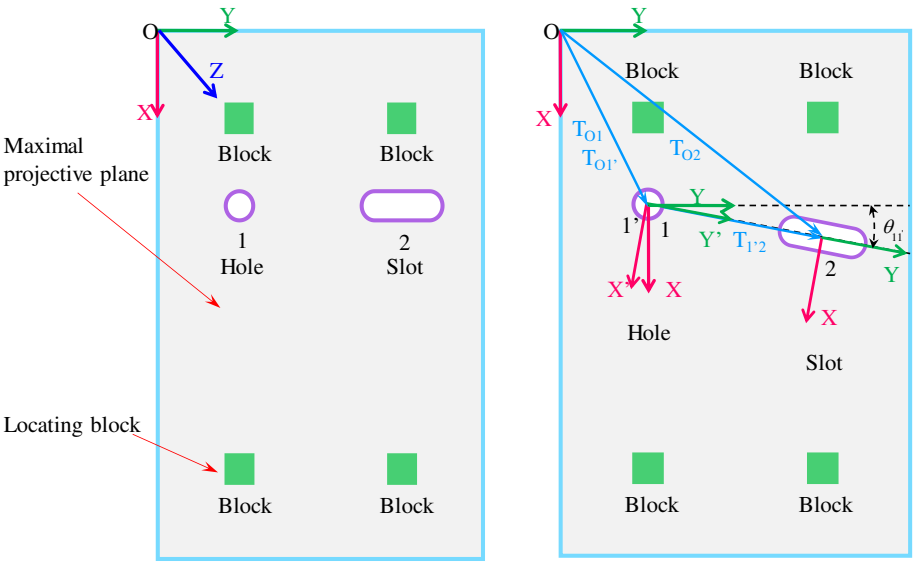

(a) Classical locating scheme of a low-rigidity structure

(b) The compound locating feature made of a hole and a slot without errors

Fig. 1 The classical locating scheme and compound locating feature without errors of a low-rigidity structure

2.2 Contributors to assembly variation of ladder structure.

For analyzing the contributors to the assembly variation of ladder structure, a simplified ladder structure constructed by two spars and five ribs is used, refer to Fig. 2(a). Since panels will be installed onto the ladder structure skeleton to form the horizontal stabilizer or the wing box, the assembly variations along the Y-axis of the observation points are paid more attention to. The observation points are denoted with pentagrams and distributed on the flanges of the spars.

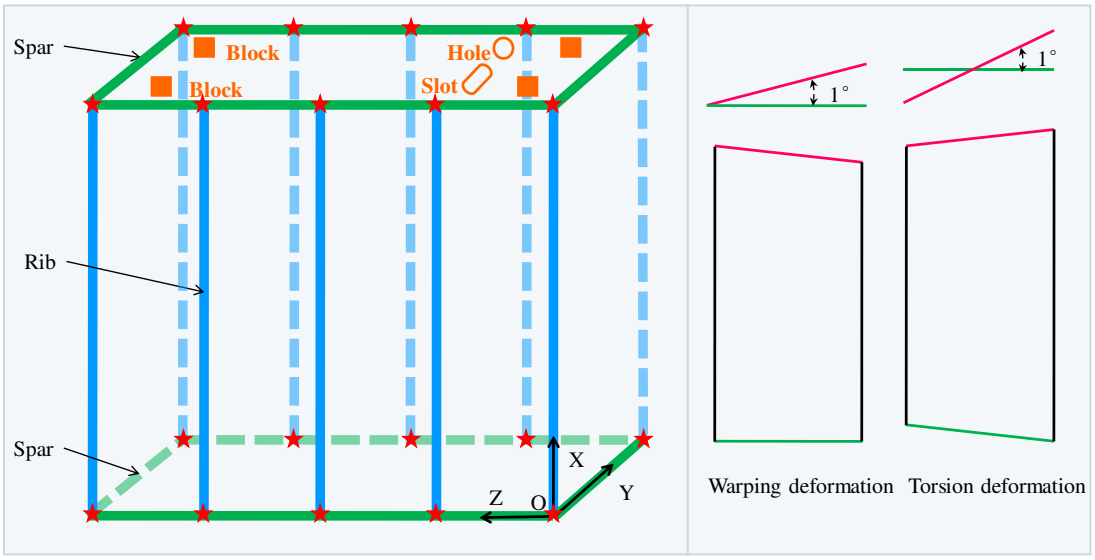

(a) Locating scheme of a simplified ladder structure

(b) An instance of representing part geometric errors with angles in top view

Fig. 2 Ladder structure locating scheme and part geometric error representing

Due to locating errors, manufacturing errors, and part deformation, an assembled part often deviates from the nominal location and geometry, which induced the assembly's dimensional variation. In the traditional mechanistic assembly variation model[7], part geometric errors of an assembled part are expressed as the deviations of key points on the part, including fastening points and observation points. However, to characterize the overall deformation of a part intuitively and reduce the complexity of the FEA and variation modeling, warping and torsion angles are used to describe the deformations of a warping part and a torsion part, respectively. An instance of representing rib deformations as warping and torsion angles is shown in Fig. 2(b).

In the assembly of the ladder structure, manufacturing errors, wear and kinematic errors of locating fixtures of the assembled parts lead to locating errors and deformations of the parts and result in the variation of the assembly. In the ladder structure shown in Fig. 2(a), locating errors related to the blocks, hole, and slot contribute to the spars' deformations and location errors. Due to the spars' flexibility along the normals of their maximal projective planes, locating errors related to the blocks along the Z-axis induce the spars' deformations along the Z-axis. Since the spars are treated as rigid-body in their maximal projective planes, locating errors related to the hole and slot lead to rigid-body kinematic errors of the spars in the maximal projective planes.

In variation modeling of the ladder structure assembly, only deformations of the ribs and locating errors of the spars in their maximal projective plane are used for constructing the assembly variation model. Locating errors related to the blocks contributes little to the ladder structure's assembly variation along the Y-axis.

3. Rigid-compliant hybrid assembly variation modeling

In this section, a rigid-compliant hybrid assembly variation model, considering rigid-body locating errors and part geometrical errors, is developed for realistic and accurate prediction of the assembly variation of the low-rigidity aircraft structure assembly.

3.1 Assembly variation induced by rigid-body locating errors.

As discussed in Section 2, only the locating errors in the spars' maximal projective planes are integrated into the estimation of the ladder structure's assembly variation. The locating errors can

be represented as the position and orientation errors of a compound locating feature made up of a hole and a slot, as shown in Fig. 1(b). It is assumed that the slot's orientation is along the line from the center of the hole to the center of the slot in the part's maximal projective plane. Frames O, 1, 2, and 1' are the part frames, the hole, the slot, and the compound feature, respectively. Transforms $\mathbf{T}_{O1}$ and $\mathbf{T}_{O1'}$ relates the hole frame 1 and the compound frame 1' to the part frame O, respectively. The difference between frames 1' and 1 is the rotation $rot(z,-\theta_{11'})$.

In Fig. 1(b), the nominal transforms $\mathbf{T}_{O1}$ and $\mathbf{T}_{O2}$, which locates the hole and slot in the part frame O, can be described as Eqs. (1) and (2), respectively.

$$\mathbf{T}_{hole\_nominal} = \mathbf{T}_{O1} = \begin{bmatrix} \mathbf{R}_{O1} & \mathbf{p}_{O1} \\ 0^T & 1 \end{bmatrix} \tag{1}$$

$$\mathbf{T}_{slot\_nominal} = \mathbf{T}_{O2} = \begin{bmatrix} \mathbf{R}_{O2} & \mathbf{p}_{O2} \\ 0^T & 1 \end{bmatrix} \tag{2}$$

Eq. (2) can be calculated by

$$\mathbf{T}_{O2} = \mathbf{T}_{O1}\mathbf{T}_{11'}\mathbf{T}_{1'2} = \mathbf{T}_{O1}\mathbf{T}_{12} \tag{3}$$

where

$$\mathbf{T}_{12} = \begin{bmatrix} \mathbf{R}_{12} & \mathbf{p}_{12} \\ 0^T & 1 \end{bmatrix} \tag{4}$$

$$\mathbf{p}_{12} = \mathbf{p}_{O2} - \mathbf{p}_{O1} = \begin{bmatrix} x_{12} \\ y_{12} \\ 0 \end{bmatrix} \tag{5}$$

And the nominal transform $\mathbf{T}_{O1'}$ locating the compound feature in the part frame O is given by

$$\mathbf{T}_{compound\_nominal} = \mathbf{T}_{O1'} = \mathbf{T}_{O1}\mathbf{T}_{11'} \tag{6}$$

where

$$\mathbf{T}_{11'} = \begin{bmatrix} \mathbf{R}_{11'} & \mathbf{p}_{11'} \\ 0^T & 1 \end{bmatrix} \tag{7}$$

$$\mathbf{p}_{11'} = 0 \tag{8}$$

In Eqs. (4) and (7), $\mathbf{R}_{11'} = \mathbf{R}_{12} = rot(z,-\theta_{11'})$

where

$$rot(z,-\theta_{11'}) = \begin{bmatrix} \cos(-\theta_{11'}) & -\sin(-\theta_{11'}) & 0 & 0 \\ \sin(-\theta_{11'}) & \cos(-\theta_{11'}) & 0 & 0 \\ 0 & 0 & 1 & 0 \\ 0 & 0 & 0 & 1 \end{bmatrix} = \begin{bmatrix} \cos\theta_{11'} & \sin\theta_{11'} & 0 & 0 \\ -\sin\theta_{11'} & \cos\theta_{11'} & 0 & 0 \\ 0 & 0 & 1 & 0 \\ 0 & 0 & 0 & 1 \end{bmatrix} \tag{9}$$

and $\cos\theta_{11'} = y_{12}/|\mathbf{p}_{12}|$, $\sin\theta_{11'} = x_{12}/|\mathbf{p}_{12}|$, $|\ |$ is the operation of calculating the length of a vector.

As shown in Fig. 3(a), due to the locating errors, the location of the compound feature could vary in the XY-plane of the part frame, which leads to the varied location of the part. The location variation of the compound feature includes the variation of the hole's position in the X- and Y-axis. The variation of the slot's orientation is denoted with the angle $\delta\theta_{11'}$ about the Z-axis, refer to Fig. 3(b). The varied locations of the hole and slot $\mathbf{T}_{hole\_varied}$ and $\mathbf{T}_{slot\_varied}$ can be expressed as

$$\mathbf{T}_{hole\_varied} = \mathbf{T}'_{O1} = \begin{bmatrix} \mathbf{R}'_{O1} & \mathbf{p}'_{O1} \\ 0^T & 1 \end{bmatrix} \tag{10}$$

$$\mathbf{T}_{slot\_varied} = \mathbf{T}'_{O2} = \begin{bmatrix} \mathbf{R}'_{O2} & \mathbf{p}'_{O2} \\ 0^T & 1 \end{bmatrix} \tag{11}$$

According to Fig. 3(b), $\mathbf{p}'_{12} = \mathbf{p}'_{O2} - \mathbf{p}'_{O1}$ is the varied vector from the locating hole to the locating slot, and

$$\delta\theta_{11'} = \cos^{-1}\left(\frac{\mathbf{p}'_{12} \bullet \mathbf{p}_{12}}{|\mathbf{p}'_{12}||\mathbf{p}_{12}|}\right) \tag{12}$$

where $\bullet$ denotes the inner product of two vectors.

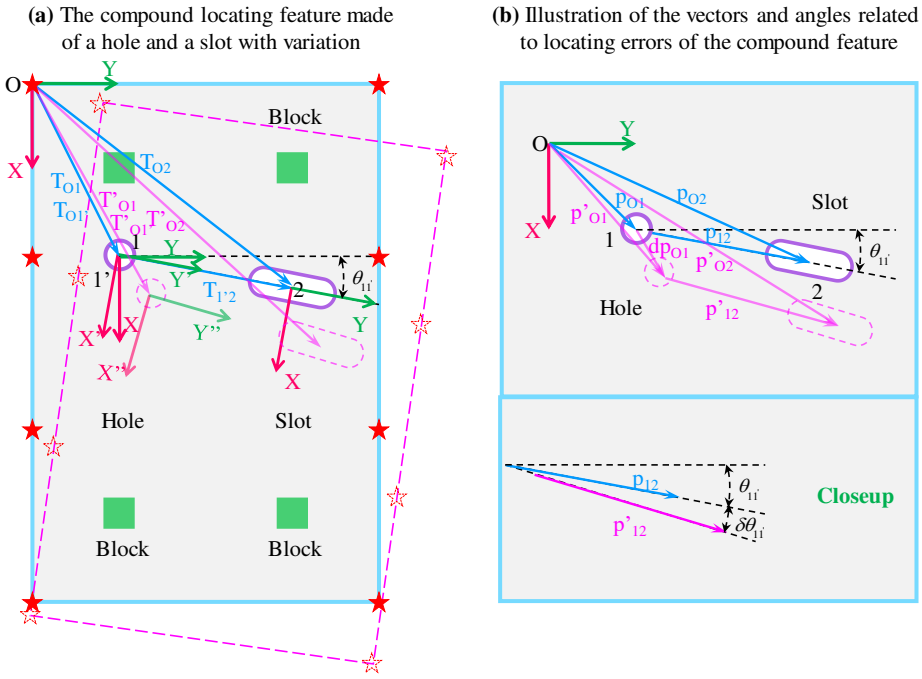

Fig. 3 The compound locating feature made of a hole and a slot with variation

The vector from the nominal locating hole to the varied hole is given by

$$d\mathbf{p}_{O1} = \mathbf{p}'_{O1} - \mathbf{p}_{O1} \tag{13}$$

Thus, we can apply Eq. (14) to obtain the varied transform $\mathbf{T}'_{O1'}$ locating the varied compound feature in the part frame O in Fig. 3(a) based on the nominal transform $\mathbf{T}_{O1'}$ and error transform $\mathbf{DT}_{O1'}$.

$$\mathbf{T}'_{O1'} = \mathbf{T}_{O1'}\mathbf{DT}_{O1'} \tag{14}$$

where

$$\mathbf{DT}_{O1'} = \begin{bmatrix} \cos(-\delta\theta_{11'}) & -\sin(-\delta\theta_{11'}) & 0 & d\mathbf{p}_{O1x} \\ \sin(-\delta\theta_{11'}) & \cos(-\delta\theta_{11'}) & 0 & d\mathbf{p}_{O1y} \\ 0 & 0 & 1 & 0 \\ 0 & 0 & 0 & 1 \end{bmatrix} = \begin{bmatrix} \cos\delta\theta_{11'} & \sin\delta\theta_{11'} & 0 & d\mathbf{p}_{O1x} \\ -\sin\delta\theta_{11'} & \cos\delta\theta_{11'} & 0 & d\mathbf{p}_{O1y} \\ 0 & 0 & 1 & 0 \\ 0 & 0 & 0 & 1 \end{bmatrix} \tag{15}$$

With small-angle approximation, Eq. (15) can be simplified as

$$\mathbf{DT}_{O1'} = \begin{bmatrix} 1 & \delta\theta_{11'} & 0 & d\mathbf{p}_{O1x} \\ -\delta\theta_{11'} & 1 & 0 & d\mathbf{p}_{O1y} \\ 0 & 0 & 1 & 0 \\ 0 & 0 & 0 & 1 \end{bmatrix} \tag{16}$$

Since the part is treated as a rigid body in its maximal projective plane, the error transform $\mathbf{DT}_{O1'}$ of the compound locating feature is the transform of the observation points distributed on the part from the nominal locations to the varied ones, as shown in Fig. 3(a). Thus position variation of the observation points, which is denoted by $\Delta\mathbf{T}_{Op}$, can be calculated by the following equations.

$$\Delta\mathbf{T}_{Op} = \mathbf{T}'_{Op} - \mathbf{T}_{Op} = \mathbf{T}_{Op}\mathbf{DT}_{O1'} - \mathbf{T}_{Op} = \mathbf{T}_{Op}(\mathbf{DT}_{O1'} - \mathbf{I}) = \mathbf{T}_{Op}\mathbf{DT}'_{O1'} \tag{17}$$

where

$$\mathbf{T}_{Op} = \begin{bmatrix} 1 & 0 & 0 & x \\ 0 & 1 & 0 & y \\ 0 & 0 & 1 & z \\ 0 & 0 & 0 & 1 \end{bmatrix}, \quad \mathbf{T}'_{Op} = \begin{bmatrix} 1 & 0 & 0 & x' \\ 0 & 1 & 0 & y' \\ 0 & 0 & 1 & z' \\ 0 & 0 & 0 & 1 \end{bmatrix}, \quad \Delta\mathbf{T}_{Op} = \begin{bmatrix} 1 & 0 & 0 & \Delta x \\ 0 & 1 & 0 & \Delta y \\ 0 & 0 & 1 & \Delta z \\ 0 & 0 & 0 & 1 \end{bmatrix} \text{ and}$$

$$\mathbf{DT}'_{O1'} = \begin{bmatrix} 0 & \delta\theta_{11'} & 0 & d\mathbf{p}_{O1x} \\ -\delta\theta_{11'} & 0 & 0 & d\mathbf{p}_{O1y} \\ 0 & 0 & 0 & 0 \\ 0 & 0 & 0 & 0 \end{bmatrix}$$

are the nominal location, varied location, location variation, and the transform between the nominal location and the location variation of the observation points in the part frame O, respectively. Thus, given the nominal locations of the observation points $\mathbf{T}_{Op}$, the position and orientation errors of the compound feature $\mathbf{DT}_{O1'}$, the position variation of the part's observation points $\Delta\mathbf{T}_{Op}$ can be obtained.

3.2 Assembly variation induced by part geometric errors.

In variation prediction of a 3D complex assembly constructed with aeronautical low-rigidity structures, e.g., the ladder structure in Fig. 2(a), the mechanistic assembly variation model[7] is often used. In the model, the sensitivity matrix $\mathbf{S}$ of assembly variation to part geometric errors related to joining areas is obtained through the FEA. Once $\mathbf{S}$ is acquired, the assembly variation induced by part geometric errors can be calculated by

$$\mathbf{u} = \mathbf{u}_0 + \mathbf{S}\mathbf{v} \tag{18}$$

where $\mathbf{u}$ is the assembly variation vector of the observation points, the initial part geometric variation vector of the observation points is denoted by $\mathbf{u}_0$, $\mathbf{v}$ is part geometric errors related to the joining areas of the assembled parts, and $\mathbf{S}$ is the sensitivity matrix.

The full expressions of the parameters in Eq. (18) are presented as

$$\mathbf{u} = \begin{bmatrix} u_1 \\ u_2 \\ \mathrm{M} \\ u_m \end{bmatrix}, \ \mathbf{u}_0 = \begin{bmatrix} u_{01} \\ u_{02} \\ \mathrm{M} \\ u_{0m} \end{bmatrix}, \ \mathbf{v} = \begin{bmatrix} v_1 \\ v_2 \\ \mathrm{M} \\ v_n \end{bmatrix}, \ \mathbf{S} = \begin{bmatrix} s_{11} & s_{12} & \mathrm{L} & s_{1n} \\ s_{21} & s_{22} & \mathrm{L} & s_{2n} \\ \mathrm{M} & \mathrm{M} & \mathrm{O} & \mathrm{M} \\ s_{m1} & s_{m2} & \mathrm{L} & s_{mn} \end{bmatrix} \tag{19}$$

where $v_1, v_2, \mathrm{L}\ , v_n$ are part deviations of n variation sources, $u_{01}, u_{02}, \mathrm{L}\ , u_{0m}$ are initial variations of the m observation points, $u_1, u_2, \mathrm{L}\ , u_m$ are the assembly variation of the m observation points, and s_{mn} is the sensitivity index of the m_{th} observation point to the n_{th} variation source.

According to Section 2.2, deformation of a rib as a low-rigidity slice structure can be characterized by warping or torsion angle. Based on this assumption, the assembly variation analysis procedure of the ladder structure in Fig. 2(a) can be described as follows:

Step (1): Design the ribs with nominal shape as well as the distorted ribs with unit-angular warping and torsion deformation by using Catia® V5R19.

Step (2): Simulate the positioning and clamping processes of a rib with warping or torsion through the FEA executed in Abaqus® 6.10.

Step (3): Model the joining process of the rib and the spars as well as the subsequent releasing process to obtain the spring back of the assembly.

Because of the assembly force induced by the exerted clamping force in step (2), the warping or torsion rib tends to be back to its initial shape after the joining and releasing processes. The displacement responses vector of the observation points to the unit-angular warping or torsion of the rib is one column of the sensitivity matrix $\mathbf{S}$.

Step (4): Repeat step (1) to step (3), and assemble the obtained displacement response vectors related to all deformation forms of the distorted ribs to obtain the sensitivity matrix $\mathbf{S}$. This matrix indicates how the assembly variations of the observation points sensitive to the warping or torsion of the ribs.

Step (5): Calculate the assembly variation vector $\mathbf{u}$ of the observation points with $\mathbf{S}$ and the initial geometric errors of the observation points $\mathbf{u}_0$.

Similar to literature[25], the positioning, clamping, fastening, and releasing processes to assembly the distorted ribs onto the spars and construct the ladder structure in Fig. 2(a) are shown in Fig. 4.

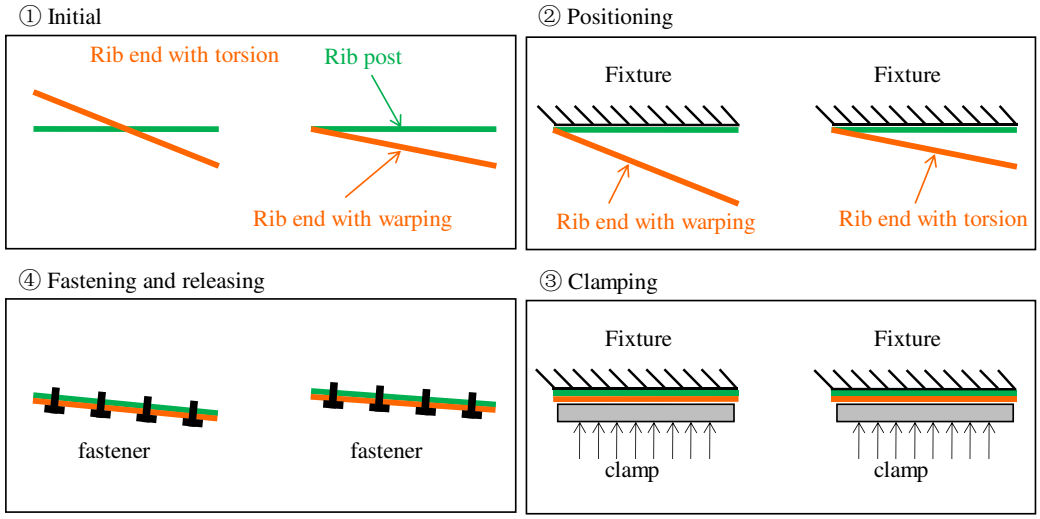

Fig. 4 Initial state, positioning, clamping, joining, and releasing of distorted ribs

3.3 A rigid-compliant hybrid variation model.

As discussed in Section 2.2, in the ladder structure assembly, the assembly variations of the observation points along the normal of the spars' flanges are paid more attention to. According to the superposition principle, the effect of the locating errors of the spars in their maximal projective planes and the influence of the part geometric errors of the ribs on the assembly variations of the observation points can be linearly superimposed. The total assembly variation of the observation points is given by

$$\mathbf{u}_{total} = \mathbf{u} + \mathbf{u}' = \mathbf{u}_0 + \mathbf{S}\mathbf{v} + \mathbf{u}' \quad (20)$$

where $\mathbf{u}'$ is the assembly variation vector of the ob

In assembly variation analysis, the MCS is often integrated with the formula of assembly variation prediction, such as Eq. (20). The initial variations of the observation points and variation sources are first sampled according to their probability distributions and then imported into the assembly variation prediction formula. Thus we can have the means and standard deviations of the assembly variations of the observation points. However, the probability distributions of the contributors to the assembly variations are sometimes unknown, especially in aircraft prototype development. Besides, a realistic situation often occurring in the industry is that the only known information about the tolerances of the assembly variations' contributors is their upper and lower bounds. To handle the problem that probability distributions of some or even all assembly variation contributors are unknown, which often occurs in variation analysis, we developed a method based on the MCS and the interval approach in Section 4.

4. Variation analysis using Monte Carlo interval approach

In this proposed variation analysis method, for the assembly variation contributors with known means and standard deviations, the MCS used in literature[7] is applied. However, for the assembly variation contributors with known tolerance bounds but unknown probability distributions, uniform sampling in the tolerance intervals is adopted. And the minimal and maximal values of the assembly variations, which are computed by using the sampling points of the contributors and the formula of assembly variation prediction, are used to construct the intervals of the assembly variations. The procedures of the proposed variation analysis method are presented in Fig. 5.

In the assembly variation analysis of the ladder structure, it is assumed that the only known information about the variation sources $d\mathbf{p}_{O1x}$, $d\mathbf{p}_{O1y}$, $\delta\theta_{11'}$, $\mathbf{v}$ is their intervals with lower and upper limits. Meanwhile, the initial variations of the observation points $\mathbf{u}_0$ follow a normal distribution (μ,σ). Thus the variation sources are treated as the interval structural parameters $dP_{O1x}=[\underline{dP_{O1x}},\overline{dP_{O1x}}]$, $dP_{O1y}=[\underline{dP_{O1y}},\overline{dP_{O1y}}]$, $\delta\Theta_{11'}=[\underline{\delta\Theta_{11'}},\overline{\delta\Theta_{11'}}]$ and $V=[\underline{V},\overline{V}]$, respectively[26, 27], and the initial variations are random numbers following (μ,σ).

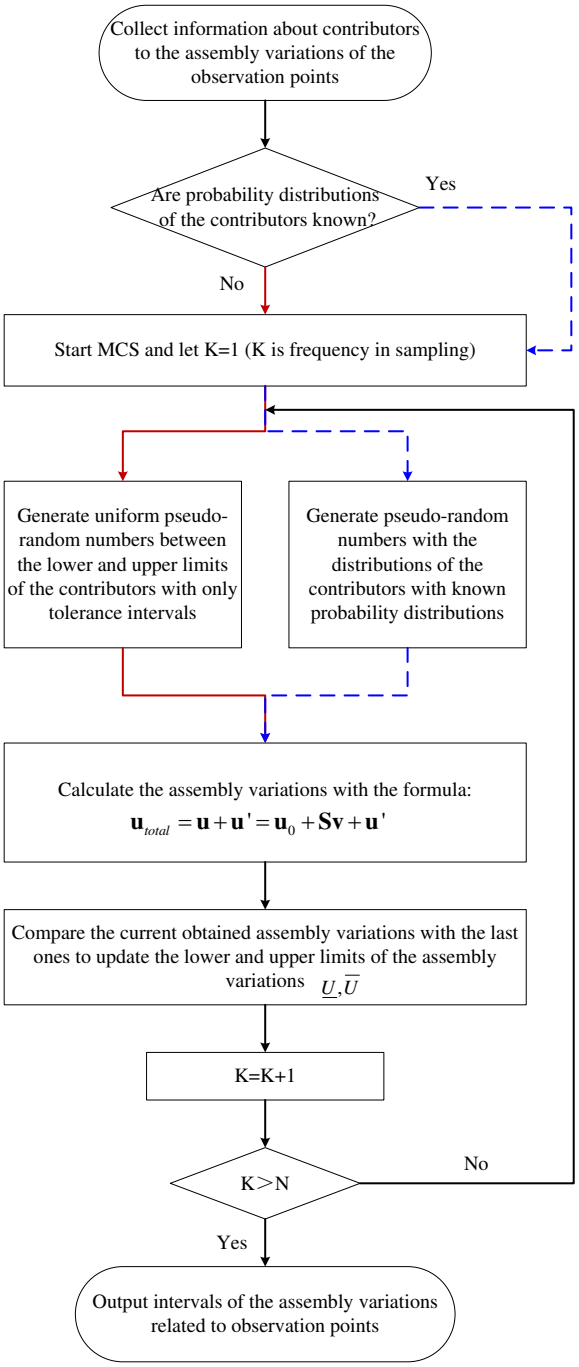

Fig. 5 Flow chart of the improved variation analysis method

In the assembly variation analysis, for the initial variations, pseudo-random numbers are generated following the known normal distributions. Meanwhile, pseudo-random numbers related to the variation sources are generated following the uniform distributions in the intervals of the variation sources' tolerances. Thus the assembly variations can be calculated by using Eqs. (17) and (20), and the sampled pseudo-random numbers related to the assembly variation contributors. The current results of the assembly variation estimation are compared with the last ones to obtain the lower and upper limits of the assembly variations. Through *N* times MCS, we can obtain the

update lower and upper limits of the assembly variations. It is evident that the results of assembly variation prediction using the proposed "Monte Carlo interval approach" are given in the form of interval structural parameters.

In the proposed method, probabilistic and non-probabilistic parameters contributing to the assembly variations can be imported into the same assembly variation prediction model. Therefore, compared with the pure MCS method, the proposed method is more universal. With the increasing of the sampling frequency, the assembly variation analysis becomes more reliable.

5. Experiments

In experiments, a simulant wing skeleton shown in Fig. 6(a) was used. The maximal cross-section of the skeleton is 850mm×600mm. The thickness of the wing skeleton and the rib spacing are all 200mm. The thickness of the ribs is 2.5mm, while the spars are 5mm in wall thickness. The spars and ribs are all manufactured with Al 2A12. The FEA of the simulant wing skeleton is executed in Abaqus® 6.10. The element type C3D8R is applied to mesh the parts, refer to Fig. 6(b).

In the assembly of the simulant wing skeleton, five contributors to the assembly variations of the observation points are considered. Twenty observation points illustrated with pentagrams in Fig. 6(a) are distributed on the skeleton to evaluate the constructed wing skeleton's quality. Among the contributors, the intervals of the warping and torsion angles of the ribs are [-3°, 3°]. The locating errors are assumed as dP_{O1x}=[-1, 1]mm, dP_{O1y}=[-1, 1]mm, and $\delta\Theta_{11'}$=[-0.5°, 0.5°]. Moreover, the initial variations of the observation points are assumed to follow the normal distribution (μ,σ)=(0, 1/3)mm. In wing box manufacturing, since the assembly of a wing skeleton is the upstream process before the assembly of wing panel onto the skeleton, the wing skeleton's assembly variation should fulfill the required tolerance for ensuring the quality of the wing box.

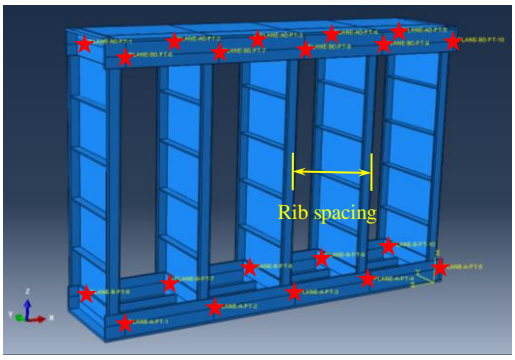

(a) The scale wing skeleton section used in experiments

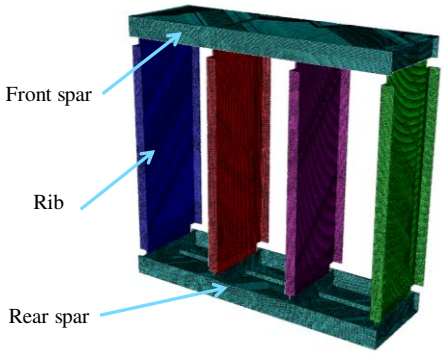

(b) The mesh model of the wing skeleton section in FEA

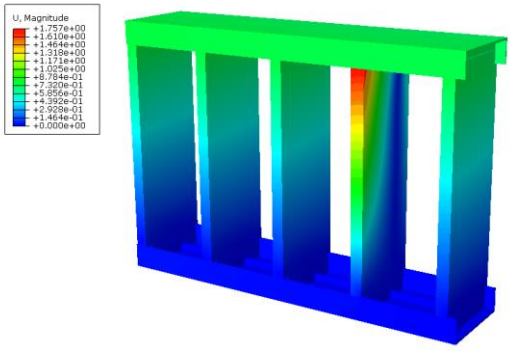

(c) The spring back simulation by the FEA

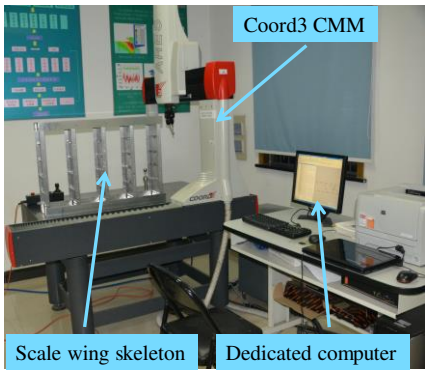

(d) The experimental platform for the wing skeleton assembly

Fig. 6 The FEA and experimental platform for the assembly of a simulant wing skeleton

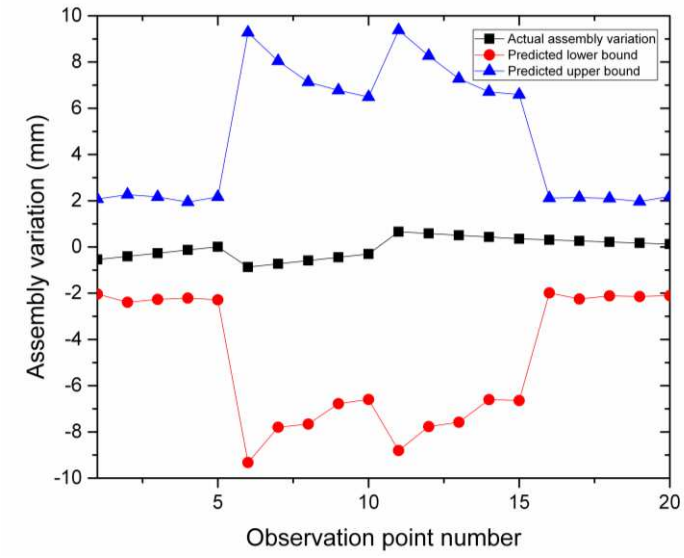

Fig. 7 The contrast of the predicted and actual assembly variations

To verify the developed hybrid assembly variation model and the proposed assembly variation analysis method based on the Monte Carlo interval approach, experiments were conducted. The results of the assembly experiment are compared with the predicted assembly variations. In the assembly variation analysis, the stress-strain relationship is supposed to be in a linear range. The experimental platform is shown in Fig. 6(c), where the assembly variations are

measured with a Coord3 coordinate measuring machine (CMM). The contrast of the assembly variations of the actual assembly and the predicted counterparts is depicted in Fig. 7. The actual results are near the middle of the intervals of the predicted ones, which indicates that the developed assembly variation model is correct, and the proposed assembly variation analysis method is efficient.

6. Conclusions

In the paper, a rigid-compliant hybrid variation analysis method using the Monte Carlo interval approach is proposed for the ladder structure assembly. The contributors to the assembly variation of a ladder structure are discussed. A concise representation of the deformation of rib structures by using the warping or torsion angle is given to reduce the complexity of the FEA and assembly variation model. The assembly variation induced by rigid-body locating errors is modeled with a homogeneous matrix and small-angle approximation. The assembly variation related to the assembled parts' geometric errors is modeled with the mechanistic assembly variation model and the FEA. Based on the two types of assembly variations, the rigid-compliant hybrid assembly variation model is established with the principle of linear superposition. The universal and improved assembly variation analysis using the Monte Carlo interval approach is proposed for dealing with the situation when the contributors' probability distributions are unknown. A case study of the assembly of a simulant wing skeleton validates the effectiveness of the developed rigid-complaint hybrid assembly variation analysis method.

Declarations

Funding

This project is supported by the National Natural Science Foundation of China (Grant No. 51805478) and the Natural Science Foundation of Fujian Province of China (No. 2020J01131). This project is also supported by the National Natural Science Foundation of China (Grant No. 51805476).

Conflicts of interest/Competing interests

The authors declare that they have no conflict of interest.

Availability of data and material

Not applicable.

Code availability

Not applicable.

Authors' contributions

Not applicable.

Ethics approval

Not applicable.

Consent to participate

Not applicable.

Consent for publication

Not applicable.

Reference

1. Chase KW, Magleby SP and Gao J. Tolerance analysis of two-and three-dimensional mechanical assemblies with small kinematic adjustments. *Advanced tolerancing techniques* 1997; 5.

2. Gao J, Chase KW and Magleby SP. Generalized 3-D tolerance analysis of mechanical assemblies with small kinematic adjustments. *IIE transactions* 1998; 30: 367-377.

3. Whitney DE. *Mechanical assemblies: their design, manufacture, and role in product development*. Oxford university press New York, 2004.

4. Huang W, Lin J, Bezdecny M, et al. Stream-of-variation modelling–Part I: a generic three-dimensional variation model for rigid-body assembly in single station assembly processes. *Journal of Manufacturing Science and Engineering* 2007; 129: 821-831.

5. HUANG W, LIN J, KONG Z, et al. Stream-of-variation (SOVA) modeling-Part II: A generic 3D variation model for rigid body assembly in multistation assembly processes. *Journal of manufacturing science and engineering* 2007; 129: 832-842.

6. Liu J, Jin J and Shi J. State space modeling for 3-D variation propagation in rigid-body multistage assembly processes. *IEEE Transactions on Automation Science and Engineering* 2009; 7: 274-290.

7. LIU S and HU S. Variation simulation for deformable sheet metal assemblies using finite element methods. *Journal of manufacturing science and engineering* 1997; 119: 368-374.

8. CAMELIO JA, HU SJ and MARIN SP. Compliant assembly variation analysis using component geometric covariance. *Journal of manufacturing science and engineering* 2004; 126: 355-360.

9. Lee B, Shalaby MM, Collins RJ, et al. Variation analysis of three dimensional non-rigid assemblies. In: *2007 IEEE International Symposium on Assembly and Manufacturing* 2007, pp.13-18. IEEE.

10. Liu SC and Hu SJ. A parametric study of joint performance in sheet metal assembly. *International Journal of machine tools and manufacture* 1997; 37: 873-884.

11. Merkley KG. *Tolerance analysis of compliant assemblies*. Citeseer, 1998.

12. Yu K, Sun J, Lai X, et al. Modeling and analysis of compliant sheet metal assembly variation. *Assembly Automation* 2008; 28: 225.

13. Dahlström S and Söderberg R. Analysis of the final geometry due to weld process effects in sheet metal assemblies. In: *Fourth International Symposium on Tools and Methods for Competitive Engineering* 2002.

14. Liu G, Huan H and Ke Y. Study on analysis and prediction of riveting assembly variation of aircraft fuselage panel. *The International Journal of Advanced Manufacturing Technology* 2014; 75: 991-1003.

15. Chang M and Gossard DC. Modeling the assembly of compliant, non-ideal parts. *Computer-aided design* 1997; 29: 701-708.

16. Aman F, Cheraghi SH, Krishnan KK, et al. Study of the impact of riveting sequence, rivet pitch, and gap between sheets on the quality of riveted lap joints using finite element method. *The International Journal of Advanced Manufacturing Technology* 2013; 67: 545-562.

17. Hu M, Lin Z, Lai X, et al. Simulation and analysis of assembly processes considering compliant, non-ideal parts and tooling variations. *International Journal of Machine Tools and Manufacture* 2001; 41: 2233-2243.

18. Camelio JA, Hu SJ and Ceglarek D. Impact of fixture design on sheet metal assembly variation. *Journal of Manufacturing Systems* 2004; 3: 182-193.

19. Hu SJ and Koren Y. Stream-of-variation theory for automotive body assembly. *CIRP Annals* 1997; 46: 1-6.

20. Camelio J, Hu SJ and Ceglarek D. Modeling variation propagation of multistation assembly systems with compliant parts. *J Mech Des* 2003; 125: 673-681.

21. Cheng H, Li Y, Zhang K-f, et al. Variation modeling of aeronautical thin-walled structures with multi-state riveting. *Journal of Manufacturing Systems* 2011; 30: 101-115.

22. Cheng H, Wang RX, Li Y, et al. modeling and analyzing of variation propagation in aeronautical thin‐walled structures automated riveting. *Assembly Automation* 2012.

23. Naing S, Burley G, Odi R, et al. Design for Tooling to Enable Jigless Assembly–An Integrated Methodology for Jigless Assembly. *SAE transactions* 2000: 299-311.

24. Vichare P, Martin O and Jamshidi J. Dimensional management for aerospace assemblies: framework implementation with case-based scenarios for simulation and measurement of in-process assembly variations. *The International Journal of Advanced Manufacturing Technology* 2014; 70: 215-225.

25. Mei B, Zhu W, Zheng P, et al. Variation modeling and analysis with interval approach for the assembly of compliant aeronautical structures. *Proceedings of the Institution of Mechanical Engineers, Part B: Journal of Engineering Manufacture* 2019; 233: 948-959.

26. Moore RE. *Methods and applications of interval analysis*. SIAM, 1979.

27. Alefeld G and Mayer G. Interval analysis: theory and applications. *Journal of computational and applied mathematics* 2000; 121: 421-464.

Figures

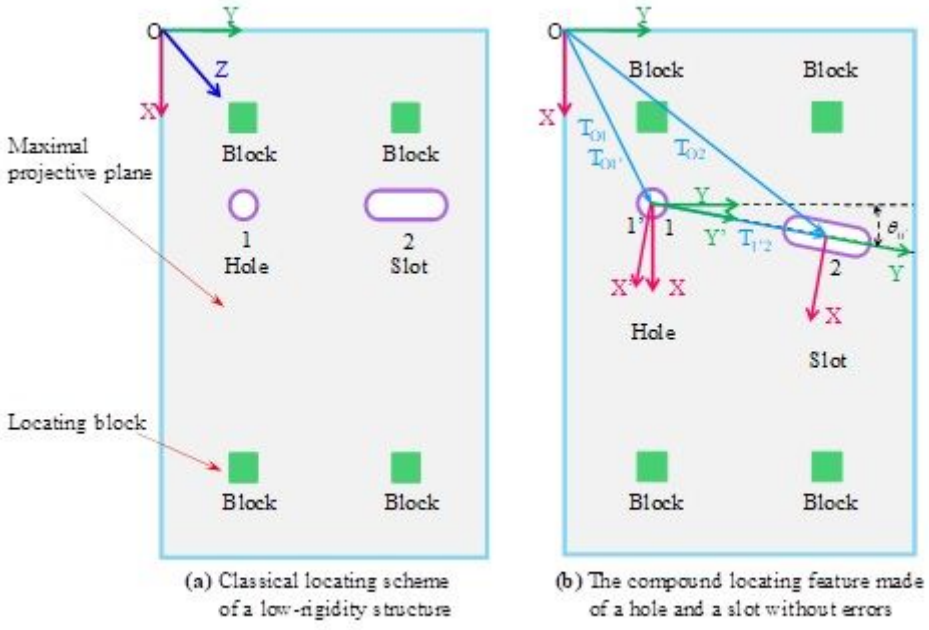

(a) Classical locating scheme of a low-rigidity structure

(b) The compound locating feature made of a hole and a slot without errors

Figure 1

The classical locating scheme and compound locating feature without errors of a low-rigidity structure

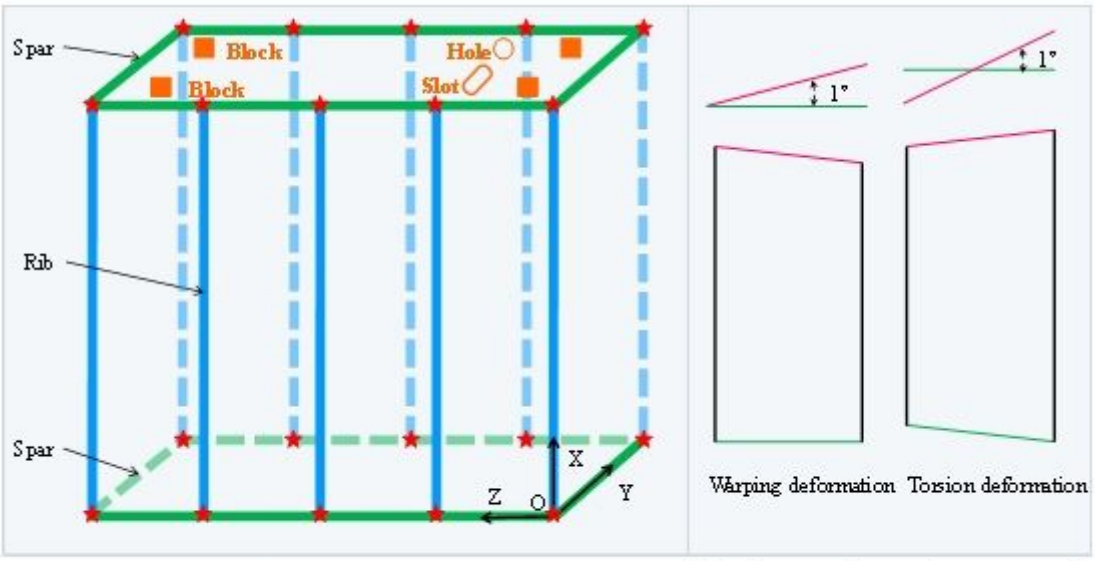

(a) Locating scheme of a simplified ladder structure

(b) An instance of representing part geometric errors with angles in top view

Figure 2

Ladder structure locating scheme and part geometric error representing

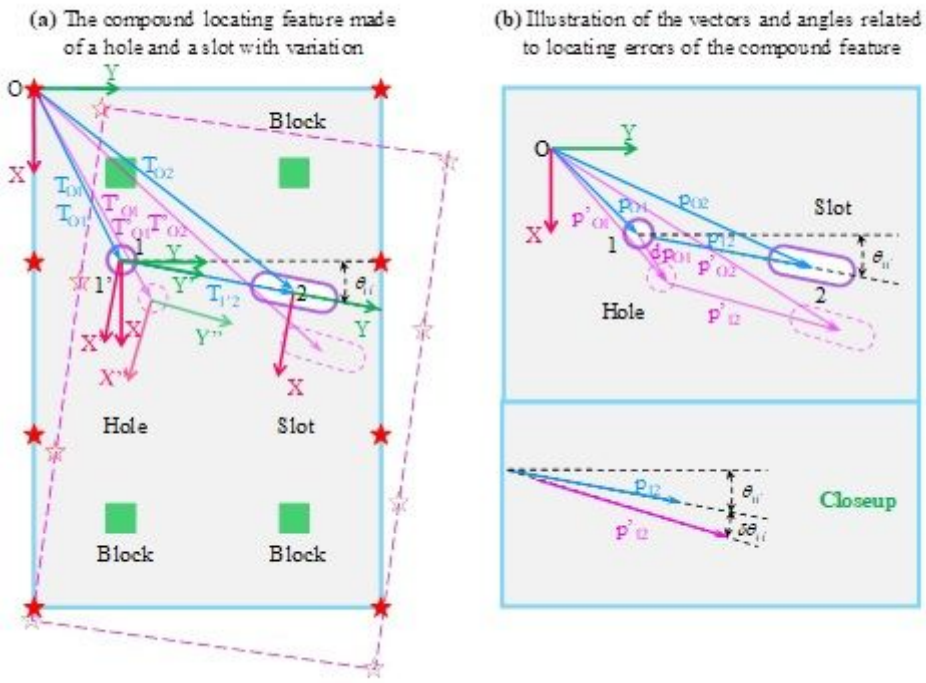

Figure 3

The compound locating feature made of a hole and a slot with variation

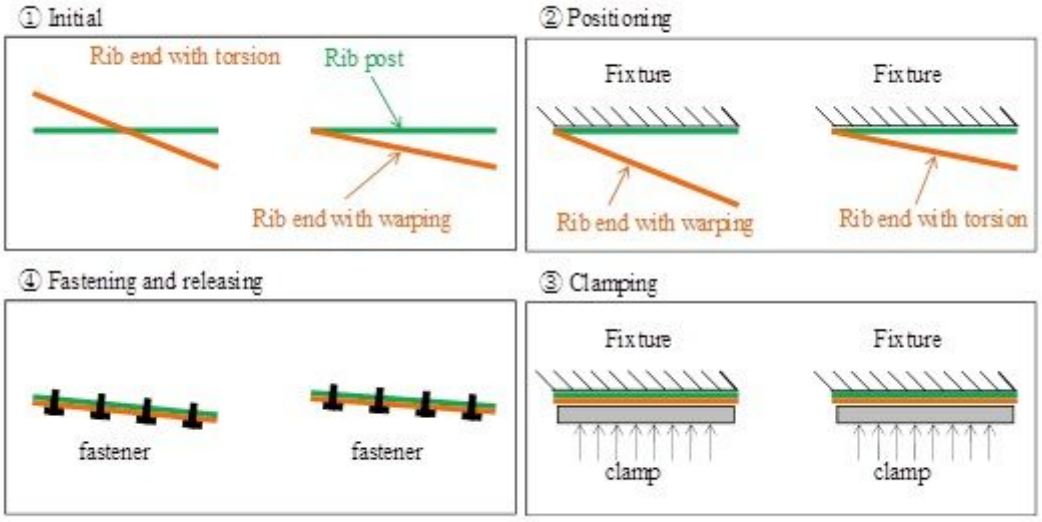

Figure 4

Initial state, positioning, clamping, joining, and releasing of distorted ribs

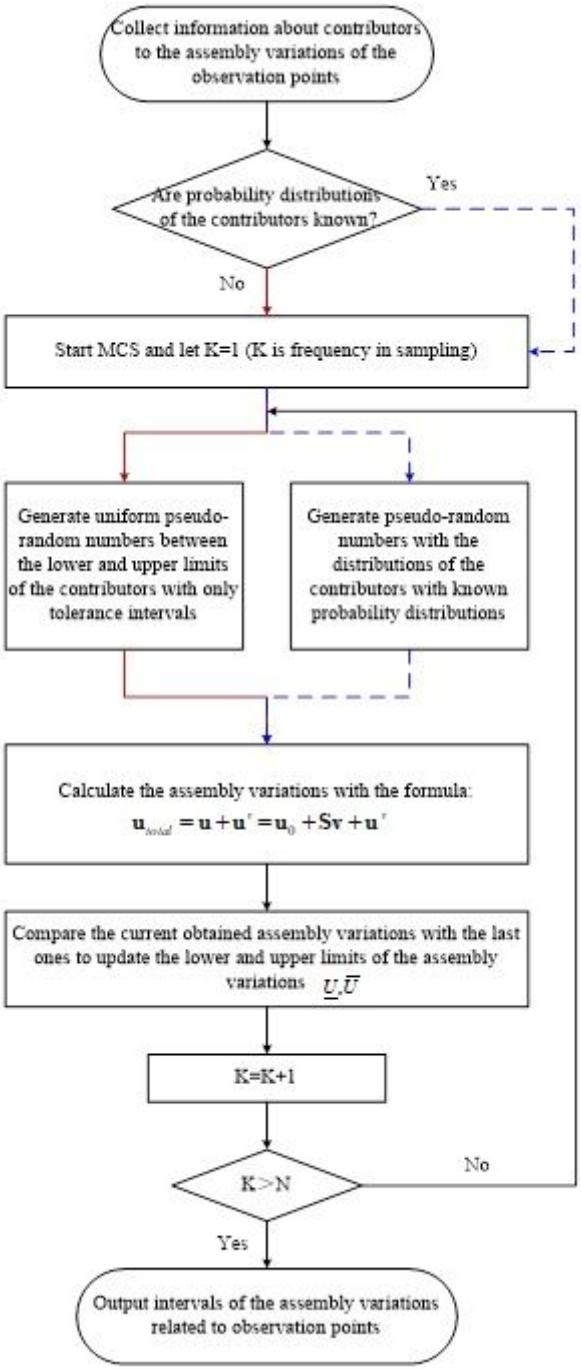

Figure 5

Flow chart of the improved variation analysis method

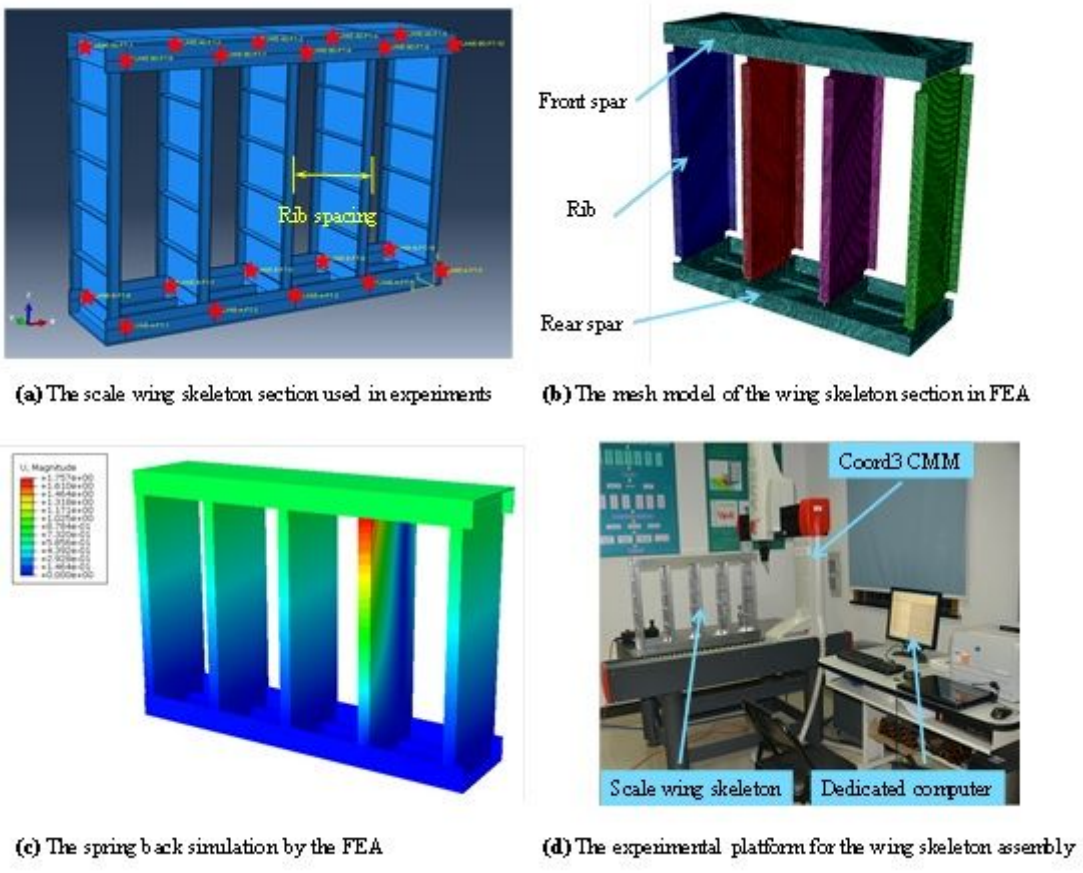

(a) The scale wing skeleton section used in experiments

(b) The mesh model of the wing skeleton section in FEA

(c) The spring back simulation by the FEA

(d) The experimental platform for the wing skeleton assembly

Figure 6

The FEA and experimental platform for the assembly of a simulant wing skeleton

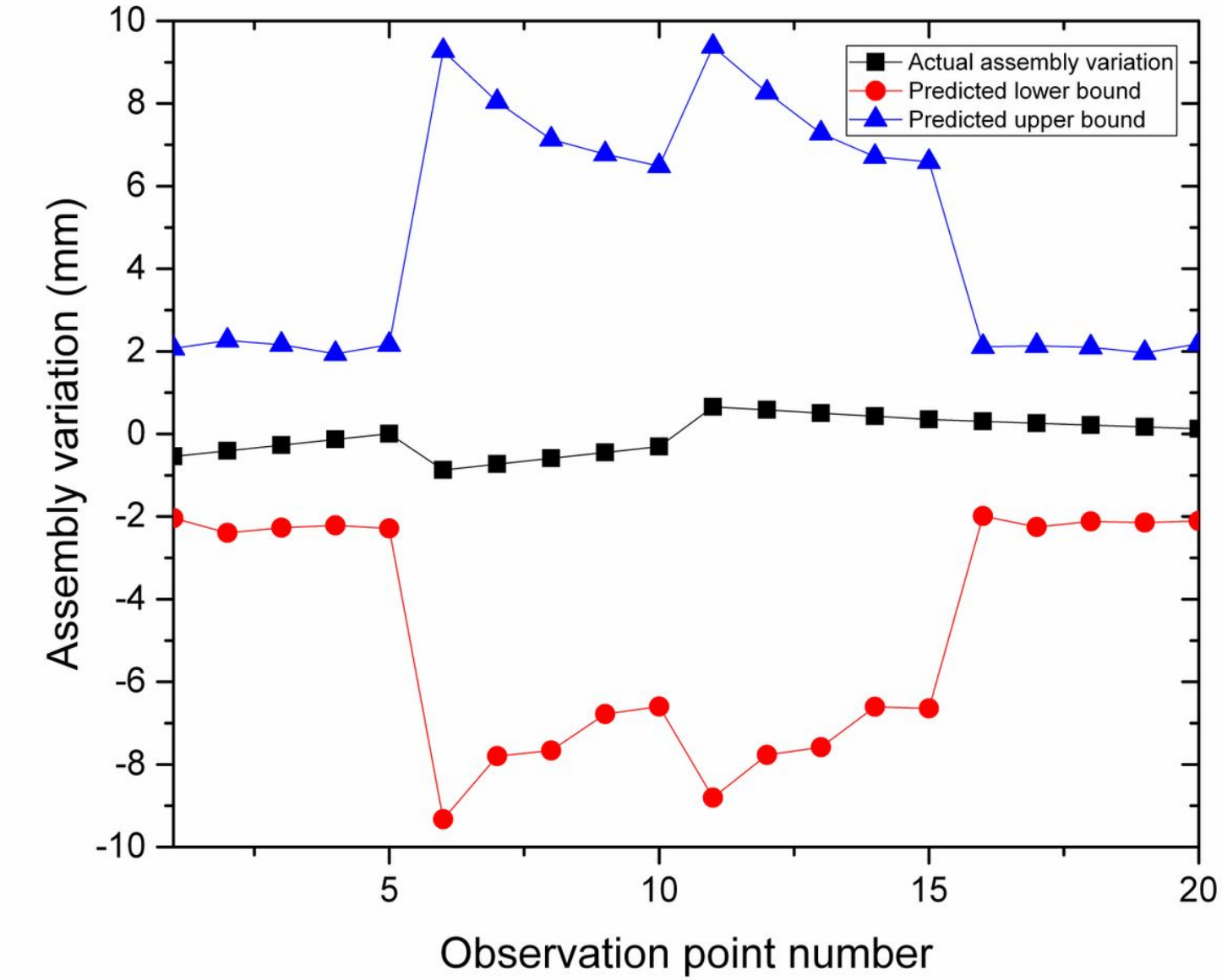

Figure 7

The contrast of the predicted and actual assembly variations